

# Femtosecond Laser Lift-Off with Sub-Bandgap Excitation for Production of Free-Standing GaN Light-Emitting Diode Chips

Steffen Bornemann,\* Nursidik Yulianto, Hendrik Spende, Yuliati Herhani, Joan Daniel Prades, Hutomo Suryo Wasisto,\* and Andreas Waag

Laser lift-off (LLO) is commonly applied to separate functional thin films from the underlying substrate, in particular light-emitting diodes (LEDs) on a gallium nitride (GaN) basis from sapphire. By transferring the LED layer stack to foreign carriers with tailored characteristics, for example, highly reflective surfaces, the performance of optoelectronic devices can be drastically improved. Conventionally, LLO is conducted with UV laser pulses in the nanosecond regime. When directed to the sapphire side of the wafer, absorption of the pulses in the first GaN layers at the sapphire/GaN interface leads to detachment. In this work, a novel approach towards LLO based on femtosecond pulses at 520 nm wavelength is demonstrated for the first time. Despite relying on two-photon absorption with sub-bandgap excitation, the ultrashort pulse widths may reduce structural damage in comparison to conventional LLO. Based on a detailed study of the laser impact as a function of process parameters, a two-step process scheme is developed to create freestanding InGaN/GaN LED chips with up to 1.2 mm edge length and  $\approx 5 \mu\text{m}$  thickness. The detached chips are assessed by scanning electron microscopy and cathodoluminescence, revealing similar emission properties before and after LLO.

management and light output of the device.<sup>[5]</sup> The latter aspect includes the development of methods to transfer functional InGaN/GaN LED layers after epitaxial growth from the sapphire substrate to different more adequate carriers, for instance, germanium wafers,<sup>[6]</sup> metal foils,<sup>[7]</sup> or flexible substrates.<sup>[8,9]</sup>

Because the fabrication of GaN substrates is complicated and therefore expensive, functional LED films are usually grown by heteroepitaxy on foreign substrates.<sup>[10]</sup> In commercial production, sapphire is often utilized because this material is readily available and compatible with GaN growth conditions.<sup>[11]</sup> However, sapphire exhibits poor electrical and thermal conductivities as well as very low optical reflectivity. Therefore, in case of highly efficient or specialized light sources, the transfer of GaN LED structures to more suitable carriers allowing a more efficient outcoupling of photons is required.


This process includes the removal of the sapphire substrate from the thin GaN layer. Up to now, various techniques have been demonstrated for this purpose, including laser lift-off (LLO),<sup>[12]</sup> grinding and dry-etching of the sapphire,<sup>[13]</sup> the use of selectively etchable<sup>[14,15]</sup> or weakly bonded intermediate layers,<sup>[16,17]</sup> natural stress-induced separation after growth,<sup>[18–21]</sup> and controlled spalling.<sup>[22]</sup>

Among these approaches, LLO has proven to be fast, efficient, and reliable.<sup>[23]</sup> In a conventional approach used today, a UV laser with pulse width in the nanosecond regime is utilized.<sup>[12,24–26]</sup>

## 1. Introduction

Due to massive advances in efficiency, durability, and versatility in the past decades, light-emitting diodes (LEDs) based on gallium nitride (GaN) are nowadays of huge importance for all kinds of visible light applications.<sup>[1–4]</sup> Their performance could be improved not only by optimizing the material quality and epitaxial structure of the InGaN/GaN layers, but also by carefully tailoring the substrate and packaging to enhance the heat

S. Bornemann, N. Yulianto, H. Spende, Dr. H. S. Wasisto, Prof. A. Waag  
Institute of Semiconductor Technology (IHT)  
Technische Universität Braunschweig  
Hans-Sommer-Straße 66, D-38106 Braunschweig, Germany  
E-mail: steffen.bornemann@tu-braunschweig.de;  
h.wasisto@tu-braunschweig.de

 The ORCID identification number(s) for the author(s) of this article can be found under <https://doi.org/10.1002/adem.201901192>.

© 2019 The Authors. Published by WILEY-VCH Verlag GmbH & Co. KGaA, Weinheim. This is an open access article under the terms of the Creative Commons Attribution License, which permits use, distribution and reproduction in any medium, provided the original work is properly cited.

DOI: 10.1002/adem.201901192

S. Bornemann, N. Yulianto, H. Spende, Dr. H. S. Wasisto, Prof. A. Waag  
Laboratory for Emerging Nanometrology (LENA)  
Technische Universität Braunschweig  
Langer Kamp 6, D-38106 Braunschweig, Germany

N. Yulianto, Dr. Y. Herhani  
Research Centre for Physics  
Indonesian Institute of Sciences (LIPI)  
Jl. Kawasan Puspiptek No. 441-442, 15314 Tangerang Selatan, Indonesia

Prof. J. D. Prades  
MIND-IN2UB  
Department of Electronic and Biomedical Engineering  
University of Barcelona  
Martí i Franquès 1, E-08028 Barcelona, Spain

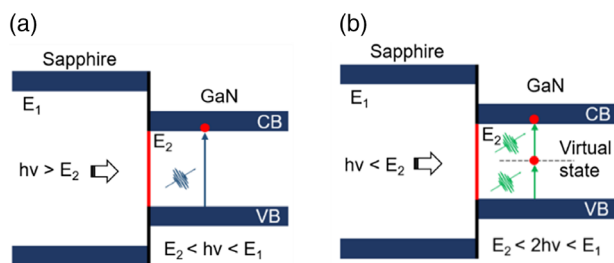


**Figure 1.** Band diagram illustrations for LLO processing of GaN on sapphire substrates. a) Conventional LLO process based on single-photon absorption. b) Two-photon absorption based on femtosecond pulses at 520 nm. The red bar indicates the zone where laser-induced ablation takes place.

The beam is directed to the backside of the LED wafer (i.e., to the transparent sapphire side; see **Figure 1a**). The photons exhibit an energy above the bandgap of GaN, so the pulse energy is dissipated at the sapphire/GaN interface. At sufficiently high pulse energies, decomposition of GaN at this interface into metallic gallium and gaseous nitrogen is induced, causing subsequent detachment of the GaN layer. The method was first demonstrated for GaN layers by Kelly et al. with the third harmonic of a Q-switched neodymium-doped yttrium aluminum garnet laser beam (355 nm).<sup>[12]</sup> Alternatively, KrF excimer lasers with 248 nm emission can be applied for LLO.<sup>[25]</sup> Nowadays, LLO has become a standard process in industrial LED production.<sup>[23]</sup> By transferring the LED layer stack to foreign carriers with tailored characteristics, for example, highly reflective surfaces, the LED performance could be drastically improved. In case of high-power LEDs, this new “thin-film LED” architecture has led to a substantial increase in light outcoupling and external quantum efficiency.<sup>[5,27]</sup>

Even though LLO is routinely used in LED fabrication, an increase in defect density due to the intense laser irradiation was proven in different studies, mainly affecting the device reverse leakage current.<sup>[28,29]</sup> Chen et al. supposed the rapid temperature increase and distribution of energy throughout the GaN layer during nanosecond laser pulses to be the main cause for crystal damage.<sup>[30]</sup> Referring to simulations, they argued that both temperature and laser-induced damage significantly decrease with reducing the pulse width.

Based on that consideration, we present a novel approach of LLO for GaN on sapphire, employing ultrashort laser pulses in the femtosecond regime. Another difference to conventional LLO is that the laser source emits at 520 nm; that is, the photon energy is lower than the GaN bandgap. Thus, linear absorption is only very small. However, the extremely high laser intensities during the ultrashort pulse times enable higher order processes, which in this case is mainly two-photon absorption (see **Figure 1b**).<sup>[31]</sup> In contrast to UV laser pulses in the nanosecond regime, light-matter interaction is not limited only to the first GaN layers. The high peak powers also trigger nonlinear processes in the sapphire, including even higher order multiphoton absorption and self-focusing.<sup>[32]</sup> Yet, in the considered intensity regime, it has been found that most of the light intensity is transmitted

through the sapphire and then absorbed at the GaN interface. The applicability of ultrashort pulses in the picosecond regime for LLO of different metal films has already been demonstrated successfully.<sup>[33]</sup> Also, the possibility of lifting functional GaN films from GaN substrates by femtosecond pulses in the infrared has been shown recently.<sup>[34]</sup> However, the application of femtosecond laser pulses in the visible wavelength regime for lift-off of GaN from sapphire is to the best of our knowledge presented here for the first time. A key advantage of our approach is that in the visible range, compact and long-lifetime solid-state lasers can be used, replacing the much more complex and costly operation of excimer lasers. Due to the short pulse width and the long wavelength, however, it involves completely different physical processes during absorption. In particular, the ultrashort time of laser–material interaction suppresses thermal effects and could therefore possibly lower the degree of thermal damage to the crystal in comparison to conventional LLO.<sup>[35,36]</sup> In contrast, the longer absorption range in case of two-photon absorption might affect layers deep inside the LED structure, especially the active area with lower bandgap.<sup>[31]</sup> It was the goal of this study to demonstrate the viability of femtosecond LLO with below-bandgap irradiation and to investigate whether this process is suitable to fabricate detached LEDs without inducing structural damage.

The proposed femtosecond lift-off process for realizing detached chips is based on a two-step procedure with varying pulse energies. The presented experiments were possible without a bonding step to a foreign wafer or tape prior to detachment. To analyze the optoelectric functionality and surface morphology after lift-off, the LED chips were assessed by scanning electron microscopy (SEM) and cathodoluminescence (CL). The results are supplemented by preparatory measurements, where the laser beam parameters in the focus region as well as the laser-induced damage threshold of GaN for the utilized laser system have been thoroughly investigated.

## 2. Results and Discussion

### 2.1. Beam Characterization and Determination of Damage Threshold for n-GaN Layers

For laser processing of GaN-based LEDs, a solid-state laser with 520 nm emission wavelength, 350 fs pulse width at a 200 kHz repetition rate, and up to 40  $\mu\text{J}$  pulse energy was utilized. It was connected to a laser machining system with a galvanometer scanner and a telecentric  $f$ -theta lens. In a first experimental series, a thorough investigation of the beam parameters in the focal region of the objective was conducted. For this purpose, plain n-GaN buffer layers were used and single laser shots were directed towards the top side of the wafer to examine the beam characteristics. The sizes of the yielded craters were assessed by SEM. According to a method proposed by Liu, the beam shape at a specific working distance of the setup can be calculated by directing single pulses at increasing energies to a test sample.<sup>[37]</sup> Assuming a Gaussian distribution with different beam widths in  $x$ - and  $y$ -direction, the planar fluence profile of the beam  $\phi(x, y)$  at the set working distance can

be described as follows, stating the laser energy per pulse and area

$$\phi(x, y) = \phi_0 \exp\left(-2\left(\frac{x^2}{\omega_x^2} + \frac{y^2}{\omega_y^2}\right)\right) \quad (1)$$

Here,  $\phi_0$  denotes the peak fluence at the center and  $\omega_x$  and  $\omega_y$  are the beam radii in  $x$ - and  $y$ -direction, respectively. Material ablation sets in as soon as the threshold fluence  $\phi_{th}$  is exceeded at any point of the surface, leaving a crater behind (see insets of **Figure 2a–c**). As can be seen in those SEM images, the shape of the crater is not circular, but rather elliptical. As expected for an astigmatic beam, the two orthogonal main axes of the ellipsis rotate by  $90^\circ$  while passing through the focal region. For a mathematical description, the coordinate system was chosen

accordingly. The  $x$  and  $y$  axes are orientated along the main axes, as shown in the inset in **Figure 2**. At the edge of a crater with diameters  $D_x$  and  $D_y$ , the fluence equals the damage threshold. Considering  $\phi\left(\frac{D_x}{2}, 0\right) = \phi\left(0, \frac{D_y}{2}\right) = \phi_{th}$  in Equation (1), it can be transformed to the following shape for both  $x$ - and  $y$ -directions

$$D_{x/y}^2 = 2 \omega_{x/y}^2 \log\left(\frac{\phi_0}{\phi_{th}}\right) \quad (2)$$

The peak fluence grows linearly with the known pulse energy  $E_p$  as

$$\phi_0 = \frac{2E_p}{\pi\omega_x\omega_y} \quad (3)$$

As  $\omega_x$  and  $\omega_y$  are constant for a defined working distance, plotting  $D^2$  against  $\ln(E_p)$  for both  $x$ - and  $y$ -directions and determining the slope leads to values for  $\omega_x$  and  $\omega_y$ , respectively. Exemplary graphs for three different working distances are depicted in **Figure 2a–c**.

For pulse energies higher than  $10 \mu\text{J}$ , the behavior deviates slightly from the linear slope in the beginning, indicating that the intensity distribution cannot be described properly with a Gaussian profile in this high-energy regime. The procedure was conducted for different relative working distances  $WD_{rel}$  around the focal region (**Figure 2e**).  $WD_{rel}$  denotes the distance of the telecentric objective from the  $z$  position, at which the geometric mean of the beam width reaches its minimum. Positive values of  $WD_{rel}$  correspond to a larger distance between objective and sample. **Figure 2e** reflects the astigmatic beam shape with minimum beam widths of  $20$  and  $26 \mu\text{m}$  for the  $x$ - and  $y$ -direction, respectively. For lift-off, the sample has to be treated on a broad area following the scanning pattern shown in **Figure 3c** so that deviations from a circular beam shape do not have a severe impact.

Furthermore, the obtained data are used to measure the laser-induced damage threshold of GaN for single-pulse irradiation, which is of importance for the lift-off process described in the next section. For each  $WD_{rel}$ , the calculated values for  $\omega_x$  and  $\omega_y$  can be reinserted into Equation (2), effectively rescaling the abscissa of the graphs in **Figure 2a–c** from pulse energy  $E_p$  to peak fluence  $\phi_0$ . The intersect of the fitted line with the  $\phi_0$ -axis, corresponding to zero crater diameter, indicates the damage threshold  $\phi_{th}$ . The obtained values are plotted in **Figure 2d**. As expected,  $\phi_{th}$  stays rather constant over the working distance, slightly deviating between  $0.4$  and  $0.55 \text{ J cm}^{-2}$ , with a mean of  $0.5 \text{ J cm}^{-2}$ . In the literature, values between  $0.25$  and  $0.9 \text{ J cm}^{-2}$  were reported for single femtosecond pulse impingement on GaN.<sup>[35,36,38,39]</sup> Ščiuka et al.<sup>[35]</sup> and Grinys et al.<sup>[38]</sup> tested the damage threshold in quite a similar regime to the one demonstrated in this work, utilizing  $515 \text{ nm}$  pulses of  $325 \text{ fs}$  width, where they measured a threshold of  $0.4 \text{ J cm}^{-2}$  for single pulses.<sup>[35,38]</sup> That value is in good agreement with the one measured in our study.

## 2.2. Lift-Off Experiments with Femtosecond Pulses

For lift-off experiments of GaN-based LEDs, the laser beam was scanned across the sample backside, that is, the sapphire side, as

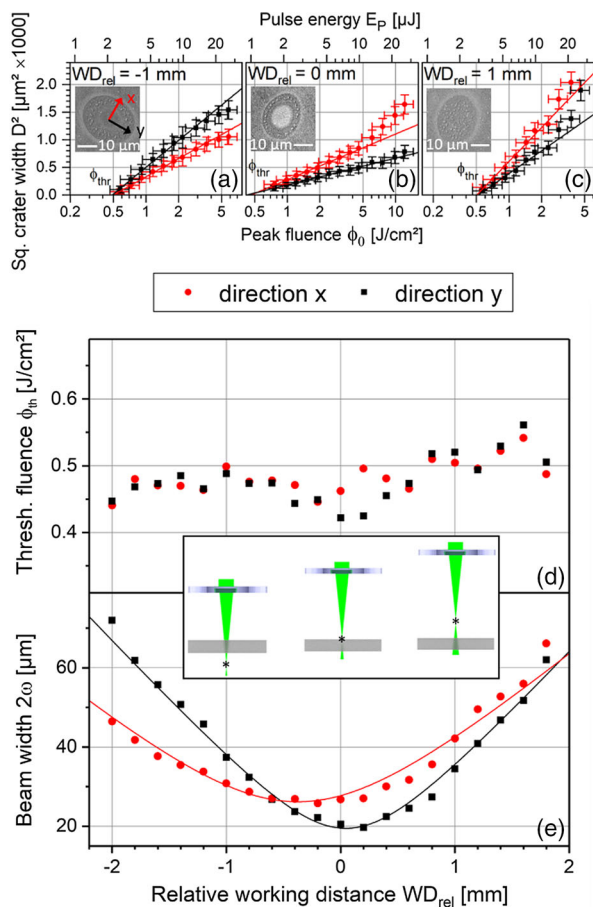


**Figure 2.** a–c) Graphs of the squared crater width against the pulse energy and peak fluence, respectively, after directing single pulses to a GaN surface at different relative working distances, that is, (a)  $WD_{rel} = -1 \text{ mm}$ , (b)  $WD_{rel} = 0 \text{ mm}$ , and (c)  $WD_{rel} = 1 \text{ mm}$ .  $x$ - and  $y$ -directions are treated separately in each case. The point where the lines intersect the lower axis corresponds to the damage threshold. The insets show SEM images of characteristic crater shapes at pulse energies of  $7 \mu\text{J}$ . In (a), the global choice of the coordinate system is illustrated. d,e) Graphs of the threshold fluence  $\phi_{th}$  and beam width  $2\omega$  in  $x$ - and  $y$ -directions in dependence on the working distance  $WD_{rel}$  around the focus position of the laser beam. The data were obtained from fit curves as depicted in (a–c). In case of the beam width, a Gaussian beam profile  $\omega = \omega_0 \sqrt{1 + ((WD_{rel} - z_0)/z_R)^2}$  was fitted to the data points for both  $x$ - and  $y$ -directions.

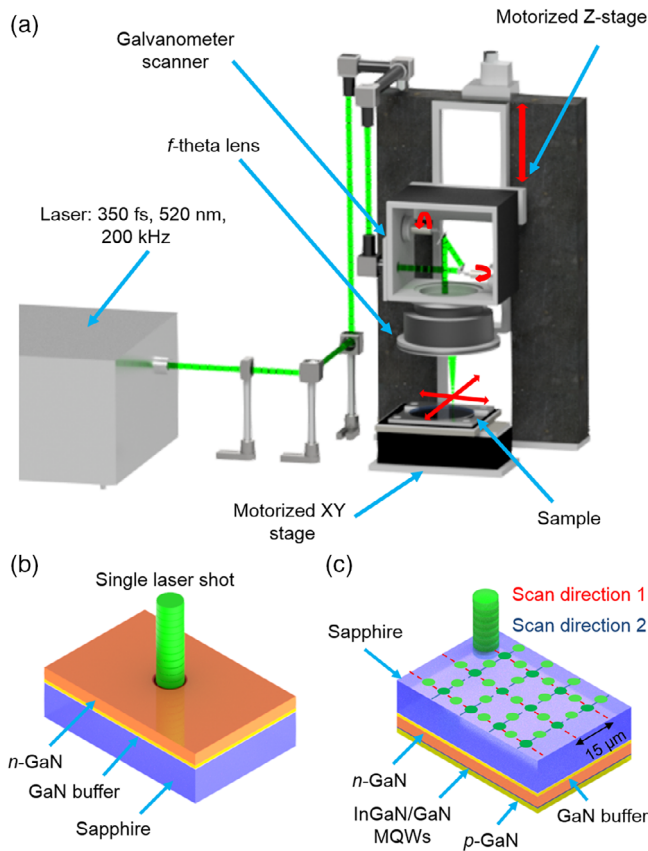


**Figure 3.** a) Sketch of the laser machining setup. The red arrows indicate freedom of movement of the corresponding devices. b, c) Sketch of laser processing in different types of experiments: (b) single shots directed to the GaN surface for analysis of the beam characteristics and (c) scanning pattern of the beam across the sapphire side in crossed lines for lift-off experiments. Green dots mark positions of impinging pulses, where darker dots are hit twice.

shown in Figure 3c. In first tests, the impact of the working distance and pulse energy was analyzed. To ensure consistent sample conditions, a two-step process was developed, as shown in Figure 4. During the first step, a GaN LED chip was defined by scanning the beam along the ring-shaped perimeter area with 100  $\mu\text{m}$  width. The width was chosen to ensure sufficient separation between the chip and its surrounding layer. However, this

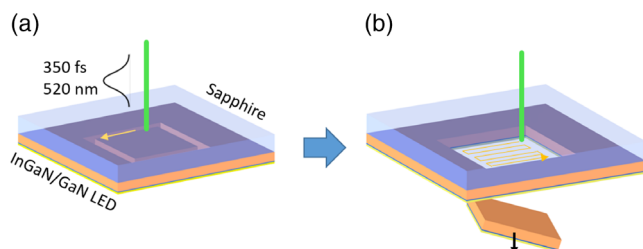


**Figure 4.** Two-step process flow for an area-selective LLO: a) high-fluence ablation for selectively creating the outer frame surrounding the to-be-lifted GaN chip and b) scanning with lower fluence for releasing the GaN chip from the sapphire substrate.

value can still be reduced to be around the according beam diameter for minimizing the wasted wafer area. For chip definition, a high pulse energy of 5  $\mu\text{J}$  was used, while the beam was scanned across the surface with the pattern shown in Figure 3c. For the tested working distance range from  $WD_{\text{rel}} = -2 \text{ mm}$  to  $WD_{\text{rel}} = 1 \text{ mm}$ , the corresponding fluence was high enough to completely remove the GaN film around the center, fragmenting it into small pieces. Subsequently, the impact of laser irradiation on the central area under different conditions was tested. The size of the chip was kept constant to  $0.5 \times 0.5 \text{ mm}^2$ . The working distance was varied between  $-2$  and  $1 \text{ mm}$  at pulse energies between  $0.7$  and  $3.3 \mu\text{J}$ . For each parameter combination, ten tests on different sites of the same wafer were conducted. In each case, the laser completed one full run through the scanning pattern. In case of a positive lift-off event, the detached film, which was facing downward, dropped onto a cover slide.

The results of this test series are shown in Figure 5a. The white numbers in the graph, at a  $x$ - $y$  position indicating the applied parameters, show how many of the ten lift-off runs had a positive outcome. For each working distance, the lift-off probability reached a maximum for a certain pulse energy. The maximum shifted to higher pulse energies when moving away from  $WD_{\text{rel}} = -0.5 \text{ mm}$ . This shift indicates that the lift-off probability is not only defined by the pulse energy and the corresponding integrated fluence  $\phi_{\text{int}} = E_p \times n/A$ , where  $n/A$  describes the number of pulses per area, but is also affected by the working distance. The influence of the working distance, that is, the beam width, is taken into consideration when regarding the peak fluence  $\phi_0$ . For each value of  $WD_{\text{rel}}$  in Figure 5, the beam widths  $\omega_{x,y}$  in  $x$ - and  $y$ -direction were computed with the fit curves from Figure 2e and then used to calculate  $\phi_0$  according to Equation (3). However, one has to consider that in case of the lift-off experiments the wafer was flipped, meaning that a sapphire

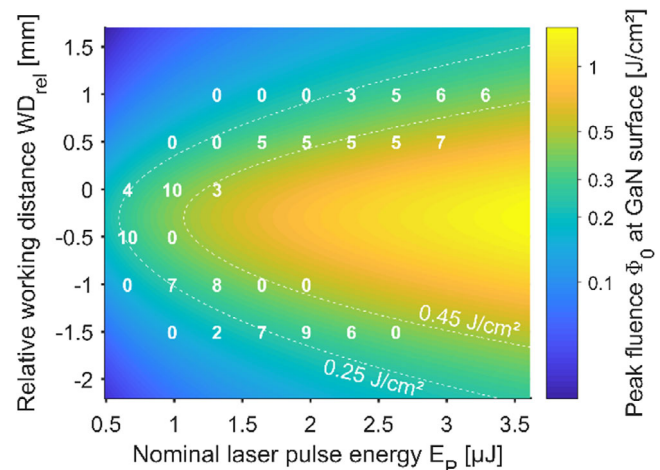


**Figure 5.** Experimental results for lift-off of GaN LED chips  $0.5 \times 0.5 \text{ mm}^2$  in size. Color-coded plot depicting the peak fluence of a laser pulse in dependence on the relative working distance and the pulse energy, calculated with the beam profile shown in Figure 2e. The white numbers in the graph indicate positive outcomes of lift-off experiments under the corresponding conditions, where ten experiments were conducted for each parameter combination.



layer with a thickness of 430  $\mu\text{m}$  had to be passed until the interface was reached. This shifted the focus position to a value of  $WD_{\text{rel}} = -0.3 \text{ mm}$ , also considering refraction of the rays at the air/sapphire interface. Moreover, Fresnel reflections at the air/sapphire and sapphire/GaN interface were considered for the calculation of the fluence values in Figure 5. In addition to those linear optical effects, nonlinear phenomena in sapphire, that is, multiphoton absorption and self-focusing, come into play for ultrashort pulses.<sup>[32]</sup> The effect of multiphoton absorption in sapphire was estimated by measuring the transmission through a double-side polished wafer without a GaN layer on top (see Figure S2, Supporting Information). It turns out that significant absorption in sapphire does not occur for the lower fluence regime, which is suitable for lift-off. Concerning self-focusing, the critical power value of  $\approx 700 \text{ kW}$  for sapphire at 520 nm is exceeded in our experiments by a factor of 3–15.<sup>[40]</sup> Thus, self-focusing might affect the pulse shape during transition through sapphire, but was not taken into account for calculating the peak fluence values displayed in Figure 5.

Despite those simplifications, Figure 5a states a quite good correlation between the lift-off probability and as-calculated peak fluence. As illustrated by the two contour lines, nearly all positive lift-off events are settled between  $\phi_0 = 0.3$  and  $0.55 \text{ J cm}^{-2}$ , defining a suitable working range for lift-off under femtosecond irradiation. In Figure 6, exemplary microscopic images of the wafer and chips after LLO are shown, fabricated at a constant working distance of  $WD_{\text{rel}} = 0.5 \text{ mm}$  and increasing pulse energies. The appearance of grayish spots on the chips is related to gallium formation at the interface (see Figure S1, Supporting Information).<sup>[25]</sup> The peak fluence in (a) is too low to induce lift-off, the chip remains at the sapphire substrate. For the highest displayed pulse energy of 2.3  $\mu\text{J}$ , the peak fluence has already

reached the upper limit of the stated interval, leading to fragmentation of the chip.

For conventional lift-off processes, the integrated fluence  $\phi_{\text{int}}$  is often given as a critical parameter.<sup>[24,25,41]</sup> In case of a non-linear process, the temporarily reached laser intensities are of more significance for the total amount of absorbed irradiation. Since the pulse width remains constant here, it seems reasonable that the reached peak fluence  $\phi_0$  is critical for lift-off. However, according to Figure 5, one might argue why LLO takes place when a peak fluence between  $\phi_0 = 0.25$  and  $0.45 \text{ J cm}^{-2}$  is reached after passing the GaN/sapphire interface, thus below the damage threshold of  $\phi_{\text{th}} = 0.5 \text{ J cm}^{-2}$  determined in the previous section. Even when taking Fresnel reflection at the GaN/air interface into consideration for the threshold fluence, the previously determined value of  $\phi_{\text{th}}$  is lowered by 17% and still reaches  $0.4 \text{ J cm}^{-2}$ . As consistently reported in the literature, there is an incubation effect, meaning that the laser-induced damage threshold is lowered if a spot on a sample is hit several times by impinging pulses.<sup>[35,38,42]</sup> This mechanism is explained by ongoing crystal modifications during repetitive laser treatment. While scanning over the surface as sketched in Figure 4b, every part of the sample was located within the beam area several times. Even if a particular spot was not in the centre of the beam, it was still reached by a significant intensity around ten times. A repetition of ten may already lower the damage threshold by a factor of  $\approx 2$ , explaining the inset of lift-off at  $\phi_{\text{th}} < 0.4 \text{ J cm}^{-2}$ . In addition, the value of the damage threshold itself might be influenced by the deviating interface conditions (i.e., for the cases of GaN/air and GaN/sapphire).

The incubation effect also explains the increasing LLO probability with a multiple number of runs through the scanning pattern. For those experiments, sample pieces were treated at  $WD_{\text{rel}} = 1 \text{ mm}$  and a laser power of 0.5 W, corresponding to a pulse energy of  $E_p = 1.6 \mu\text{J}$ . Looking at Figure 5, those conditions are not sufficient for lift-off, as the peak fluence only reaches  $0.19 \text{ J cm}^{-2}$ . After several runs through the pattern, lift-off could be achieved (see Figure S3, Supporting Information). However, it has to be mentioned that the probability of the lift-off was highly site-specific in this case.

Taking the scanning pattern presented in Figure 3c into consideration, the integrated fluences  $\phi_{\text{int}}$  for the presented lift-off method can be calculated. For a single scan over the surface, the integrated fluences in case of positive lift-off events vary between 1 and  $5 \text{ J cm}^{-2}$ . These values are considerably higher than the integrated fluences reported for conventional lift-off,<sup>[24,25,29]</sup> ranging from 0.1 to  $1 \text{ J cm}^{-2}$ . This seems reasonable, as the absorption probability in case of two-photon excitation in GaN is lower than for conventional LLO.<sup>[31]</sup> Thus, a considerable fraction of the pulses travel further into and even through the semiconductor. However, ablation takes place in the first GaN layers, as is proven by the positive lift-off events and also further demonstrated in the next section.

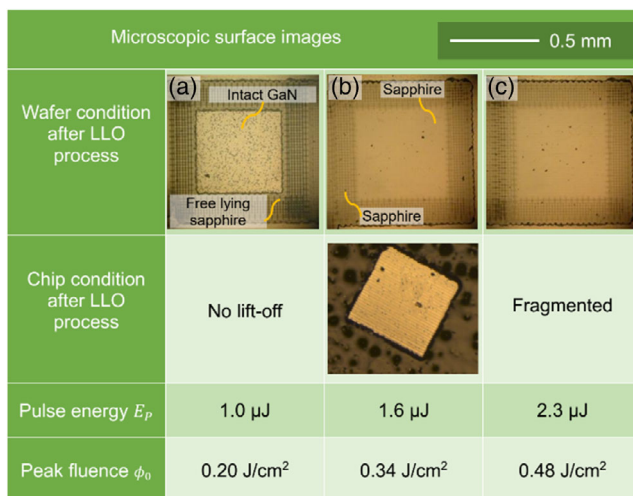


**Figure 6.** Microscopic images of the wafer and chip surface after applying the two-step LLO process depicted in Figure 4 with increasing laser power. The relative working distance  $WD_{\text{rel}}$  was kept constant at 0.5 mm. a) The energy was too low to initialize lift-off and the chip remained on the wafer. b) For  $0.3 \text{ J/cm}^2 < \phi_0 < 0.45 \text{ J cm}^{-2}$ , the lift-off regime was reached as shown in (b,c). c) A higher peak fluence of  $\approx 0.5 \text{ J cm}^{-2}$  has already led to fragmentation in this case.

### 2.3. Characterization of Lifted LED Chips

During lift-off, the detached LED chips directly dropped onto a cover slip, so that both their p- and n-GaN surfaces were

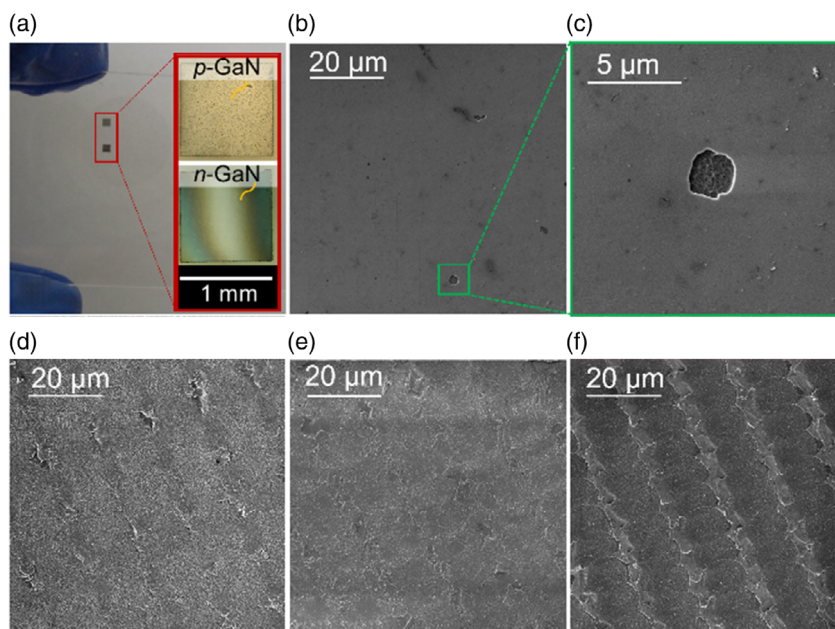


**Figure 7.** a) Freestanding GaN chips of edge length 1 mm with magnified view of the p- and n-GaN side. b,c) Secondary electron (SE) map of the p-GaN side, chip with 0.5 mm edge length lifted at  $0.34 \text{ J cm}^{-2}$ . d–f) SE maps of the n-GaN side with growing peak fluence: (d)  $0.19 \text{ J cm}^{-2}$ , five runs, (e)  $0.26 \text{ J cm}^{-2}$ , one run, and (f)  $0.34 \text{ J cm}^{-2}$ , one run.

accessible for further investigation (Figure 7a). The p-GaN surface of a lifted chip looked smooth (Figure 7b), except for some scattered areas where the p-GaN layer had been blown off (see Figure 7c). Since those areas did not occur on the wafer before lift-off, they were a consequence of the laser irradiation. As discussed before, the light penetrates deeper into the crystal in case of two-photon absorption. Consequently, a considerable fraction of the remaining light might be absorbed at indium-rich spots in the multiple-quantum well (MQW),<sup>[43]</sup> leading to local ablation of the p-GaN layer above. In terms of the density of the surface defects, its value depends on several factors (e.g., the condition of the employed wafer, the laser energy, and the number of repetitions through the pattern). Thus, it can strongly vary from process to process. In one case, densities of up to  $10^5 \text{ cm}^{-2}$  were found, whereas in other cases they were not detectable at all. Thus, the surface defect densities are approximated to be in the range of  $0\text{--}10^5 \text{ cm}^{-2}$  after LLO. To understand the underlying reasons of these variations, more LLO experiments and surface characterizations are required in future. In Figure 7d–f, the n-GaN surfaces of chips that were lifted at different peak fluences are shown. In Figure 7d,e, the peak fluence is rather low, with  $0.19$  and  $0.26 \text{ J cm}^{-2}$ , respectively. The n-GaN surface looks comparatively smoother after ablation (also compare to Figure S4, Supporting Information). In contrast, the chip lifted at a higher peak fluence of  $0.34 \text{ J cm}^{-2}$  has a rough interface, where the laser scanning pattern can easily be recognized. For further processing of the chip, a smooth surface is required. Thus, working at lower peak fluences in the given interval should be preferred.

Moreover, cross sections of both the wafer before LLO and the detached chips were analyzed, as shown in Figure 8a,b,

respectively. The breaking edge was produced by locally pressing onto the chip on the carbon pad. In both cases, the measured film height ranged from  $5.5$  to  $5.8 \mu\text{m}$ . This implies that only the first layer at the interface was destroyed during ablation, which is similar to the case of conventional LLO.

As indicated by the panchromatic CL map (Figure 8b), there was still bright emission from the MQW region of the detached chip. The main emission wavelength at  $\approx 500 \text{ nm}$ , which resulted from the MQW, remained constant after LLO (Figure 8c). There was another small peak at  $\approx 385 \text{ nm}$ , which also stemmed from the MQW region. This is indicated by constraining the CL scan area to small regions at the cross section (Figure 8d). This peak was already present before LLO. Most probably, it originated from a thin InGaN phase with indium content of a few percent underneath the MQW region, grown to reduce the threading dislocation density in the active area. Around  $365 \text{ nm}$ , the near band edge emission of GaN caused another peak in the CL spectra, which was significantly higher in case of the untreated wafer. Even though a quantitative analysis of CL intensities is generally difficult as many parameters have an impact on the signal intensity, the two curves in Figure 8c show a quite similar behavior. Thus, the CL data imply stable emission properties of the LED layer after femtosecond LLO, with bright illumination from the MQW (also see Figure S5 and S6, Supporting Information). LED devices with according metal contacts have not been processed yet, so that electrical characterization has not been performed so far. However, these issues will be investigated and tackled for the next generation of LED devices manufactured with femtosecond LLO processing.

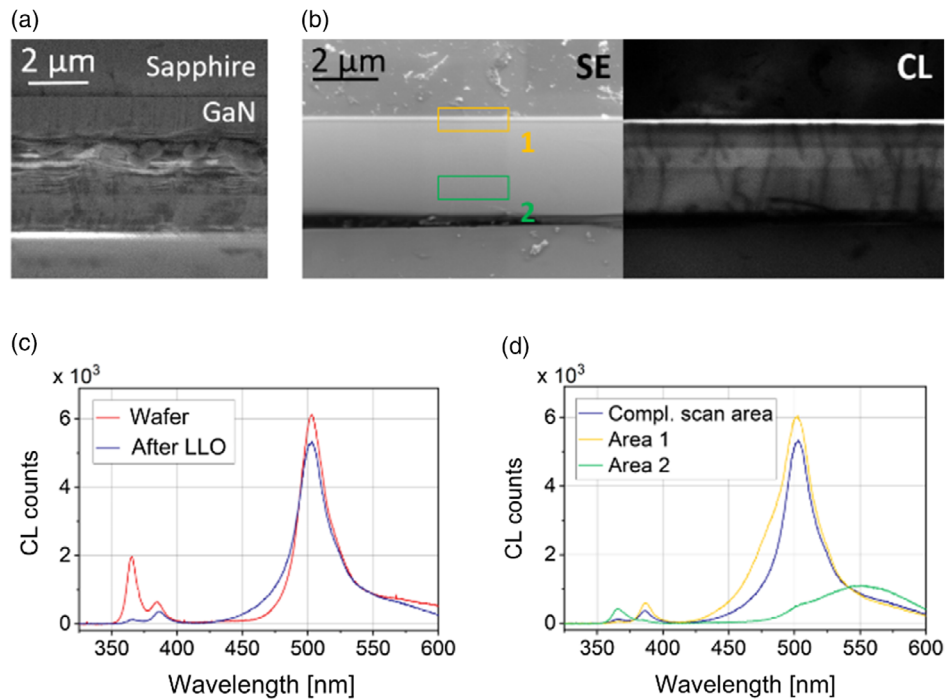


**Figure 8.** a) Cross-sectional SE map of the GaN LED wafer before LLO, revealing a thickness of  $\approx 5.8 \mu\text{m}$ . b) SE map of a tilted edge ( $30^\circ$ ) of a lifted chip with a corresponding panchromatic CL signal obtained at 5 kV electron energy and a beam current of 250 pA. The breaking edge was produced by pressing onto the chip. Bright MQW emission as well as threading dislocations inside the GaN layer, visible as dark vertical lines, can be seen. c) CL spectra, acquired at 10 kV and 250 pA, comparing emission from the cross sections as shown in (a,b). d) CL spectra obtained from different scan areas shown in (b), acquired at 10 kV and 250 pA.

### 3. Conclusion

The feasibility of applying femtosecond laser pulses at a wavelength of 520 nm for LLO of GaN-based LED films from sapphire substrates has successfully been demonstrated in this article. In preparatory measurements, the beam characteristics of the used laser system have carefully been investigated and a laser-induced damage threshold of  $0.5 \text{ J cm}^{-2}$  for GaN has been determined. For LLO, the beam is scanned over the sapphire side of the sample in a quadratic pattern. Significant multiphoton absorption occurs in the vicinity of the GaN/sapphire interface. The peak fluence at the GaN/sapphire interface has been identified as the critical parameter, which must range between approximately  $0.25$  and  $0.45 \text{ J cm}^{-2}$  for lift-off. This interval is slightly below the measured damage threshold, which can be explained by taking the incubation effect into consideration. The integrated fluence during femtosecond LLO is well above  $1 \text{ J cm}^{-2}$ , that is, higher than for conventional LLO, which is expected due to the nonlinear nature of absorption. A key question is whether below-bandgap light causes damage to the GaN layers. The optical quality of the MQWs before and after LLO has been found to be comparable, indicating that the MQWs or GaN layers do not experience damage. However, an impact of laser irradiation on small localized areas in the p-GaN has been found, indicating a higher absorption at these “hot spots.” The underlying mechanism and effects on LED performance have to be further explored. A two-step recipe has been developed to create free-standing GaN LED chips with variable sizes up to 1.2 mm edge

length. SEM measurements indicate that the roughness of the n-GaN surface is affected by the applied peak fluence during lift-off, whereas the GaN layer thickness does not change considerably during detachment. It can be concluded that the presented femtosecond LLO is a viable alternative approach to lift GaN-based LEDs from sapphire. Key advantages are that our approach relies on solid-state lasers instead of excimer lasers and that our technique is less dependent on the bandgap of the semiconductor material. Therefore, it should be possible to even detach AlN layers from sapphire substrates using femtosecond LLO techniques.<sup>[31]</sup> For AlN, the realization of an efficient lift-off process has proven to be difficult with conventional LLO.<sup>[44]</sup>

### 4. Experimental Section

**Wafer Design:** In the presented experiments, two types of wafers were utilized, that is, plain n-GaN layers of roughly  $\approx 4 \mu\text{m}$  thickness for laser beam characterization and InGaN/GaN LED structures for demonstration of LLO. Both types of samples were epitaxially grown on  $430 \mu\text{m}$  thick 2" sapphire substrates by metalorganic vapor-phase epitaxy (MOVPE) inside an Aixtron G3 reactor in an in-house epitaxy competence center (ec<sup>2</sup>). The InGaN/GaN films with a total thickness of  $\approx 5 \mu\text{m}$  consisted of a  $2.4 \mu\text{m}$  thick low-doped n-GaN buffer layer, a  $2.1 \mu\text{m}$  heavily doped n-GaN layer with a dopant density of  $10^{18}$ – $10^{19} \text{ cm}^{-3}$ , four pairs of InGaN/GaN MQWs, and a p-GaN layer with a total thickness of  $\approx 300 \text{ nm}$ . The LED epilayers were grown on double-side polished sapphire substrates to facilitate light transmission from the backside.

**Laser Micromachining:** The experimental setup for conducting the femtosecond LLO is sketched in Figure 3a. The laser source emits at a center

wavelength of 520 nm with a pulse width of 350 fs and a repetition rate of 200 kHz. It comprises an internal pulse picker. The laser beam is guided towards a micromachining stage by several mirrors. The stage consists of a galvanometer scanner with an attached telecentric  $f$ -theta objective and a sample holder. The distance between the objective and the sample, that is, the working distance, can be adapted by vertical movement of the galvanometer scanner with a motorized precision stage. The mirrors inside the scanner allow fast  $xy$  beam scanning along the sample surface with velocities up to  $2 \text{ m s}^{-1}$ , where the angle of incidence onto the surface is kept orthogonal by the telecentric objective. Moreover, additional  $xy$  movement is provided by two linear positioners underneath the sample holder. The optical transmissivity of the laser machining system was measured to be 0.83. The  $f$ -theta objective enables fast sample processing with constant beam parameters over a plane area as large as  $40 \times 40 \text{ mm}^2$ . A large focal length of  $f = 100 \text{ mm}$  is required for this, connected to a rather high Rayleigh length of  $\approx 1 \text{ mm}$ .

In first preparatory experiments, single laser pulses were directed toward plain  $n$ -GaN layers, without passing through the sapphire, as depicted in Figure 3b. Sufficient lateral distance of  $150 \mu\text{m}$  between two pulses was provided by scanning the beam along a line with the galvanometer scanner at a speed of  $1 \text{ m s}^{-1}$  and setting the pulse picker to 30. Resulting craters on the semiconductor surface for different working distances and pulse energies were measured inside a field emission scanning electron microscope equipped with a customized CL detection setup. For the lift-off of LED chips, the focused beam was scanned across the sample on a selected area with the galvanometer scanner. The applied pattern is illustrated in Figure 3c. The area was scanned in orthogonal lines with  $15 \mu\text{m}$  distance. As the scanning velocity and the repetition rate were  $1.5 \text{ m s}^{-1}$  and 200 kHz, the distance between two impinging pulses along a scanned line was  $7.5 \mu\text{m}$ . Depending on the working distance, the beam width of the laser was at least  $20 \mu\text{m}$  (see Figure 2). Thus, the scanning pattern ensured a homogeneous treatment of the surface.

## Supporting Information

Supporting Information is available from the Wiley Online Library or from the author.

## Acknowledgements

S.B. and N.Y. contributed equally to this work. This work was funded in part by the Lower Saxony Ministry for Science and Culture (N-MWK) within the group of "LENA-OptoSense" and in part by the European Union's Horizon 2020 research and innovation program within the project of "ChipScope – Overcoming the Limits of Diffraction with Super-Resolution Lighting on a Chip" under grant agreement no 737089. The authors would like to thank C. Margenfeld and I. Mangano Clavero for sample preparation in the epitaxy competence centre (ec<sup>2</sup>). N.Y. thanks the Ministry of Research, Technology and Higher Education of the Republic of Indonesia (RISTEKDIKTI) for the Ph.D. scholarship of Riset-Pro under no. 345/Riset-Pro/FGS/VIII/2016 and the Indonesian-German Centre for Nano and Quantum Technologies (IG-Nano) for the support. J.D.P. acknowledges the support from the Serra Hünter Program and the ICREA Academia Program of the Government of Catalonia as well as the DFG Project GrK NanoMet.

## Conflict of Interest

The authors declare no conflict of interest.

## Keywords

femtosecond laser, GaN, laser lift-off, light-emitting diodes, nonlinear optics

Received: October 2, 2019

Revised: November 16, 2019

Published online:

- [1] S. Li, A. Waag, *J. Appl. Phys.* **2012**, *111*, 5.
- [2] J. Herrnsdorf, J. J. D. McKendry, S. Zhang, E. Xie, R. Ferreira, D. Massoubre, A. M. Zuhdi, R. K. Henderson, I. Underwood, S. Watson, A. E. Kelly, E. Gu, M. D. Dawson, *IEEE Trans. Electron Devices* **2015**, *62*, 1918.
- [3] G. Scholz, Q. Xu, T. Schulze, H. Boht, K. Mattern, J. Hartmann, A. Dietzel, S. Scherneck, I. Rustenbeck, J. Prades, S. Fündling, H. Wasisto, A. Waag, *Proceedings* **2017**, *1*, 552.
- [4] N. Markiewicz, O. Casals, C. Fabrega, I. Gràcia, C. Cané, H. Suryo Wasisto, A. Waag, J. D. Prades, *Appl. Phys. Lett.* **2019**, *114*, 53508.
- [5] A. Laubsch, M. Sabathil, J. Baur, M. Peter, B. Hahn, *IEEE Trans. Electron Devices* **2010**, *57*, 79.
- [6] V. Haerle, B. Hahn, S. Kaiser, A. Weimar, S. Bader, F. Eberhard, A. Plössl, D. Eisert, *Phys. Status Solidi A* **2004**, *201*, 2736.
- [7] H. Kuo, S. Wang, P. Wang, K. Uang, T. Chen, S. Chen, W. Lee, H. Hsu, J.-C. Chou, C. Han Wu, *IEEE Photonics Technol. Lett.* **2008**, *20*, 523.
- [8] C. Goßler, C. Bierbrauer, R. Moser, M. Kunzer, K. Holc, W. Pletschen, K. Köhker, J. Wagner, M. Schwaerzle, P. Ruther, O. Paul, J. Neef, D. Keppeler, G. Hoch, T. Moser, U. T. Schwarz, *J. Phys. D: Appl. Phys.* **2014**, *47*, 205401.
- [9] B. Damilano, M. Lesecq, D. Zhou, E. Frayssinet, S. Chenot, J. Brault, N. Defrance, A. Ebongue, Y. Cordier, V. Hoel, *IEEE Photonics Technol. Lett.* **2018**, *30*, 1567.
- [10] G. Li, W. Wang, W. Yang, Y. Lin, H. Wang, Z. Lin, S. Zhou, *Rep. Prog. Phys.* **2016**, *79*, 056501.
- [11] B. Park, R. S. Kumar, M. Moon, M. Kim, T. Kang, W. Yang, S. Kim, *J. Cryst. Growth* **2015**, *425*, 149.
- [12] M. K. Kelly, O. Ambacher, R. Dimitrov, R. Handschuh, M. Stutzmann, *Phys. Status Solidi A* **1997**, *159*, R3.
- [13] S. Zhou, S. Liu, *Appl. Surf. Sci.* **2009**, *255*, 9469.
- [14] J. Ha, S. W. Lee, H. Lee, H. Lee, S. H. Lee, H. Goto, T. Kato, K. Fujii, M. W. Cho, T. Yao, *IEEE Photonics Technol. Lett.* **2008**, *20*, 175.
- [15] T. Tsai, R. Horng, D. Wu, S. Ou, M.-T. Hung, H. H. Hsueh, *Electrochem. Solid-State Lett.* **2011**, *14*, 434.
- [16] J. Kim, C. Bayram, H. Park, C. Cheng, C. Dimitrakopoulos, J. A. Ott, K. B. Reuter, S. W. Bedell, D. K. Sadana, *Nat. Commun.* **2014**, *5*, 1.
- [17] T. Ayari, S. Sundaram, X. Li, Y. El Gmili, P. L. Voss, J. P. Salvestrini, A. Ougazzaden, *Appl. Phys. Lett.* **2016**, *108*, 171106.
- [18] K. Ohnishi, M. Kanoh, T. Tanikawa, S. Kuboyu, T. Mukai, T. Matsuoka, *Appl. Phys. Express* **2017**, *10*, 1.
- [19] A. S. Altkhov, R. I. Gorbunov, L. A. Kasharina, F. E. Latshev, *Tech. Phys. Lett.* **2016**, *42*, 1076.
- [20] K. Yamane, M. Ueno, H. Furuya, N. Okada, K. Tadatomo, *J. Cryst. Growth* **2012**, *358*, 1.
- [21] A. D. Williams, T. D. Moustakas, *J. Cryst. Growth* **2007**, *300*, 37.
- [22] S. W. Bedell, C. Bayram, K. Fogel, P. Lauro, J. Kiser, J. Ott, Y. Zhu, D. Sadana, *Appl. Phys. Express* **2013**, *6*, 1.
- [23] R. Delmdahl, R. Pätzelt, J. Brune, *Phys. Procedia* **2013**, *41*, 241.
- [24] W. S. Wong, T. Sands, N. W. Cheung, M. Kneissl, D. P. Bour, P. Mei, L. T. Romano, N. M. Johnson, *Appl. Phys. Lett.* **1999**, *75*, 1360.
- [25] T. Ueda, M. Ishida, M. Yuri, *Jpn. J. Appl. Phys.* **2011**, *50*, 1.
- [26] J. Kim, J. H. Kim, S. H. Cho, K. H. Whang, *Appl. Phys. A: Mater. Sci. Process.* **2016**, *122*, 1.
- [27] B. Hahn, B. Galler, K. Eng, *Jpn. J. Appl. Phys.* **2014**, *53*, 100208.
- [28] Y. Sun, T. Yu, H. Zhao, X. Shan, X. Zhang, Z. Chen, X. Kang, D. Yu, G. Zhang, *J. Appl. Phys.* **2009**, *106*, 1.
- [29] J.-H. Cheng, Y. S. Wu, W. C. Peng, H. Ouyang, *J. Electrochem. Soc.* **2009**, *156*, H640.



- [30] M. Chen, J. Y. Zhang, X. Q. Lv, L. Y. Ying, B. P. Zhang, *Chinese Phys. Lett.* **2013**, 30, 1.
- [31] C.-K. Sun, J.-C. Liang, J.-C. Wang, F.-J. Kao, S. Keller, M. P. Mack, U. Mishra, S. P. DenBaars, *Appl. Phys. Lett.* **2000**, 76, 439.
- [32] G. Eberle, M. Schmidt, F. Pude, K. Wegener, *Appl. Surf. Sci.* **2016**, 378, 504.
- [33] G. Heise, M. Domke, J. Konrad, S. Sarrach, J. Sotropa, H. P. Huber, *J. Phys. D: Appl. Phys.* **2012**, 45, 1.
- [34] V. Voronenkov, N. Bochkareva, R. Gorbunov, A. Zubrilov, V. Kogotkov, P. Latyshev, Y. Lelikov, A. Leonidov, Y. Shreter, *Results Phys.* **2019**, 13, 27.
- [35] M. Ščiuka, T. Grinys, M. Dmukauskas, V. Plerpaitė, A. Melninkaitis, *Jpn. J. Appl. Phys.* **2013**, 52, 08JK08-1.
- [36] W. M. Liu, R. Y. Zhu, S. X. Qian, S. Yuan, G. Y. Zhang, *Chinese Phys. Lett.* **2002**, 19, 1711.
- [37] J. M. Liu, *Opt. Lett.* **1982**, 7, 196.
- [38] T. Grinys, M. Dmukauskas, M. Ščiuka, S. Nargelas, A. Melninkaitis, *Appl. Phys. A: Mater. Sci. Process.* **2014**, 114, 381.
- [39] P. G. Eliseev, S. Juodkazis, T. Sugahara, H.-B. Sun, S. Matsuo, S. Sakai, H. Misawa, *Proc. SPIE* **2000**, 4065, 546.
- [40] S. Juodkazis, K. Nishimura, S. Tanaka, H. Misawa, E. G. Gamaly, B. Luther-Davies, L. Hallo, P. Nicolai, V. T. Tikhonchuk, *Phys. Rev. Lett.* **2006**, 96, 1.
- [41] R. Delmdahl, R. Pätzel, J. Brune, R. Senczuk, C. Goßler, R. Moser, M. Kunzer, U. T. Schwarz, *Phys. Status Solidi A* **2012**, 209, 2653.
- [42] J. Bonse, J. M. Wrobel, J. Krüger, W. Kautek, *Appl. Phys. A: Mater. Sci. Process.* **2001**, 72, 89.
- [43] Y. Lin, K. Ma, C. Hsu, S. Feng, Y.-C. Cheng, C.-C. Liao, C. C. Yang, C.-C. Chou, C.-M. Lee, J.-I. Chyi, *Appl. Phys. Lett.* **2000**, 77, 2988.
- [44] H. K. Cho, O. Krüger, A. Külberg, J. Rass, U. Zeimer, T. Kolbe, A. Knauer, S. Einfeldt, M. Weyers, M. Kneissl, *Semicond. Sci. Technol.* **2017**, 32, 1.